MSc in Photonics

PHOTONICS**BCN**

Universitat Politècnica de Catalunya (UPC)
Universitat Autònoma de Barcelona (UAB)
Universitat de Barcelona (UB)
Institut de Ciències Fotòniques (ICFO)

http://www.photonicsbcn.eu

Master in Photonics

MASTER THESIS WORK

Attosecond X-ray Transient Dynamics

Jorge Delgado Guerrero

Supervised by Dr. Antonio Picón, (ICFO)

Presented on 8th September 2017

Registered at

Escola Tècnica Superior d'Enginyeria de Telecomunicació de Barcelona

Attosecond X-Ray Transient Dynamics

Jorge Delgado Guerrero[1]

[1] Attoscience and Ultrafast Optics Group. The Institute of Photonic Sciences (ICFO). Mediterranean Technology Park, Av. Carl Friedrich Gass, 3, 08860. Castelldefels, Barcelona, Spain
jorgedelguerrero@gmail.com

Abstract. We present a theoretical approach for studying the dynamics in semiconductor materials induced by intense IR laser pulses by using the absorption of an attosecond x-ray pulse. We develop the theory and study three physical scenarios: a three-level atomic system, a three-band semiconductor system with no intraband interactions, and a three-band semiconductor system taken into account all interactions. For each system, we calculate the corresponding attosecond transient absorption (ATA), that is, the change of the absorption of the system due to the dynamical response induced by the IR pulse. We show the possibility to track electron carriers by using x-ray ATA spectroscopy and anticipate some difficulties at high IR intensities.

Keywords: attosecond transient absorption, semiconductors, ultrafast optics

1. Introduction

The need to observe and visualize the different phenomena that are under study, is key for the advance of science and the development of novel applications. For example, the necessity of seeing objects that are too small for the human eye gave birth to the microscope, which led to many advances in different fields of science. Following this example, nowadays we find instruments such as atomic force microscopes or techniques such as x-ray crystallography which allow us to get clear pictures of individual atoms and molecules. However the great spatial resolution provided by these instruments cannot be extended with comparable temporal resolution.

Since the invention of the laser (Malman, 1961), the laser technology advances made significant progress, and nowadays it is feasible to obtain high intensity pulses with few femtosecond (10^{-15} s) duration. This gave birth to femtochemistry (1980s) [1], a revolutionary field that studies chemical reactions on extremely short timescales for which A.H. Zewail was awarded with the Nobel Prize. The leading technique of this field is the well-known pump-probe spectroscopy (figure 1). In this technique two pulses are used: pump pulse and probe pulse. The pump pulse is responsible for exciting the system, and triggering the dynamics that we want to study, whereas the probe pulse is a delayed pulse which is used to probe the pump-induced dynamics. By repeating the experiment many times at different delays between the two pulses, we build a sequence of pictures which allow us to observe and study the dynamics of interest. Since fs scale corresponds to the realm of atomic vibrations, femtochemistry allows to perform measurements of

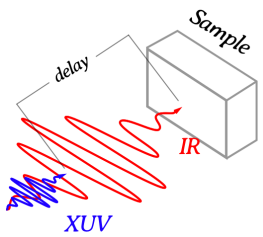

Figure 1. Pump-probe scheme with a pump IR pulse and a probe XUV pulse

vibrational motions in such a way that chemical reactions can almost be followed in real time. Despite the achievements in this field, which represented an important step forward in our understanding of light-induced phenomena in matter, the upcoming of the twenty-first century gave rise to a new breakthrough in the field of time-resolved studies: the reach of the attosecond realm.

1.1. Attosecond science

Since the beginning of the 2000s the capability of producing attosecond pulses (10^{-18} s), which was the next frontier in time resolved experiments, is a reality. The advent of attosecond pulses opens the door to explore electron dynamics, which offers the possibility to observe, and perhaps to control of the rapid motion of electrons in different systems.

Attosecond pulses are generated as follows: a NIR fs pulse is focused on a target material, which generates attosecond light pulses via high harmonic generation (HHG). In this process, the NIR pulse distort the atomic potential giving rise to tunneling ionization, then the electron wavepacket is releaased into the continuum and accelerated away. Then, by changing the sign of the electric field, the electrons are accelerated back towards the parent ion to collide with it. From the inelastic recollision, the excess of kinetic energy is released as brief attosecond light bursts, whose frequency is in the XUV domain (odd-harmonic of the NIR originial frequency) [2].

Due to the intrinsic synchronization between the IR and the XUV pulse, different attosecond metrology and spectroscopy techniques have been developed. From these techniques, we are interested in the attosecond transient absorption (ATA) technique, which is based on a pump-probe technique. The idea is to determine the absorption spectrum of the attosecond pulse for different delays between the NIR pulse (pump pulse) and the XUV pulse (probe pulse). The NIR pulse is delayed by using a variable delay stage, and then it is focus along with the XUV pulse into the sample. By means of a grating spectrometer, the XUV spectra is recorded onto a x-ray CCD camera. The same experience is repeated with and without pulse, and by measuring the changes in absorption between both spectra we are able to retrieve the information of the induced dynamics [2].

A great promise is the realization of ATA studies with attosecond "x-ray" pulses. This represents an important step for performing spectroscopy studies in the water windows, relevant for many physical, chemical, and biological processes. Within this context, our group has been able of generating for the first time isolated soft-x-ray attosecond pulses [3]. This achievement has opened novel prospects for spectroscopy applications but also a new and never-considered domain of light matter-interaction where theory will play an important role [4]. Besides, the study of ultraintense laser fields with matter has been mainly focused on atomic and molecular gases, and much less literature is found for condensed matter systems. Here, we present a work in which theoretical and computational tools have been developed in order to understand future ATA experiments performed on semiconductor materials and might have a high impact in this field.

2. Theory

The theory that describes our system is based on semiconductor Bloch equations (SBE), a standard model for semiconductor optical physics. To model our system, we consider a system with N-level electronic bands in which conduction and valence bands are coupled via IR laser. Since we

deal with periodic systems, Bloch functions are used to describe the wavefunction of the bands, distinguishing between the ground state electronic level ($|\mathbf{k}, g\rangle$) and the first excited electronic levels ($|\mathbf{k}, \lambda\rangle$) [5]:

$$|\psi(\mathbf{r}, t)\rangle = \int d\mathbf{k}^3 a_g(\mathbf{k}, t)|\mathbf{k}, g\rangle + \sum_\lambda \int d\mathbf{k}^3 a_\lambda(\mathbf{k}, t)|\mathbf{k}, \lambda\rangle \tag{1}$$

The size of the electron is small compared to the wavelength of the electromagnetic field, which means that we can apply the so-called *dipole approximation* (vector potential only depends on time $\mathbf{A}(\mathbf{r_o}, t) = \mathbf{A}(t)$). Under this assumption, we write the Schrödinger equation in the length Gauge as follows:

$$i\hbar \frac{\partial}{\partial t}\psi^{LG}(\mathbf{r}, t) = \left[\hat{H}_e - \sum_j q_j \mathbf{r}_j \cdot \boldsymbol{\varepsilon}(t)\right] \psi^{LG}(\mathbf{r}, t) \tag{2}$$

where the interaction term is defined as $\hat{V}_I(t) = -\sum_j q_j \mathbf{r}_j \cdot \boldsymbol{\varepsilon}(t)$, being $\boldsymbol{\varepsilon}(t)$ the electric field. We derive the equation of the dynamics of our system substituting the Ansatz (1) in equation (2), by considering the dipole transition [5]

$$\langle \mathbf{k}', a|\hat{V}_I(t)|\mathbf{k}, b\rangle \approx -i\boldsymbol{\varepsilon}(t) \cdot \frac{\partial}{\partial \mathbf{k}}[\delta(\mathbf{k} - \mathbf{k}')\, \delta_{ab}] + i \int d\mathbf{r}^3 e^{-i(\mathbf{k}'-\mathbf{k})\mathbf{r}} u^*_{\mathbf{k}',a}(\mathbf{r})\, \boldsymbol{\varepsilon}(t) \cdot \frac{\partial}{\partial \mathbf{k}} u_{\mathbf{k},b}(\mathbf{r}) \tag{3}$$

where a, b correspond to different Bloch functions. The first term of the right-hand-side of (3) is different than zero only if we have intraband coupling. If this is the case, the second term of the equation can be neglected. On the contrary, when we have interband coupling, the first term is necessarily zero. Besides, using the so-called **kp** theory, it can be proved that the interband coupling term is only different than zero when we have vertical transitions [5], therefore: $\langle \mathbf{k}, \lambda|\hat{V}_I(t)|\mathbf{k}', \lambda'\rangle = \boldsymbol{\varepsilon}(t) \cdot \mathbf{d}_{\lambda\lambda'}(\mathbf{k})$. In the bands of a semiconductor electrons are found in mixed states rather than in pure states. Thus, we use the density matrix formalism which is constructed by $\rho_{ij} = a_i^\dagger(\mathbf{k}, t) a_j(\mathbf{k}, t)$. If $\hat{H}_{eff}|\mathbf{k}, a\rangle = E_a(\mathbf{k})|\mathbf{k}, a\rangle$, we have:

$$\begin{aligned}
i\,\dot{\rho}_{ij}(\mathbf{k}, t) &= [E_j(\mathbf{k}) - E_i(\mathbf{k}) - i\frac{1}{T_2}]\, \rho_{ij}(\mathbf{k}, t) + \\
&\sum_{\lambda' \neq j} \boldsymbol{\varepsilon}(t) \cdot \mathbf{d}_{j\lambda'}(\mathbf{k})\, \rho_{i\lambda'}(\mathbf{k}, t) - \sum_{\lambda' \neq i} \boldsymbol{\varepsilon}(t) \cdot \mathbf{d}^*_{i\lambda'}(\mathbf{k})\, \rho_{\lambda' j}(\mathbf{k}, t) + i\boldsymbol{\varepsilon}(t) \cdot \frac{\partial}{\partial \mathbf{k}} \rho_{ij}(\mathbf{k}, t) \\
i\,\dot{\rho}_{ii}(\mathbf{k}, t) &= -i\frac{1}{T_1}\rho_{ii}(\mathbf{k}, t) + 2\,i\,\mathrm{Im}[\sum_{\lambda' \neq i} \boldsymbol{\varepsilon}(t) \cdot \mathbf{d}_{i\lambda'}(\mathbf{k})\, \rho^\dagger_{\lambda' i}(\mathbf{k}, t)] + i\boldsymbol{\varepsilon}(t) \cdot \frac{\partial}{\partial \mathbf{k}} \rho_{ii}(\mathbf{k}, t)
\end{aligned} \tag{4}$$

where we use $\rho_{i\lambda'} = \rho^\dagger_{\lambda' i}$. The first equation is related to the coherence between two electron bands, while the second equation is related to the population in a particular band. The added parameters $-\frac{1}{T_1}$ and $-\frac{1}{T_2}$ are relaxation and dephasing terms which represents phenomena such as thermalization effects, electron-phonon scattering, or electron-electron correlations.

So far, the formalism that we have developed is focused on the interaction of the system with a strong optical laser. Nevertheless, we want to implement time-resolved experiments with an IR pump pulse and a x-ray probe pulse. We express the electric field as a sum of both pulses: $\boldsymbol{\varepsilon}(t) = \boldsymbol{\varepsilon}_o(t) + \boldsymbol{\varepsilon}_x(t)$ (o is used to describe the optical pulse and x is used for the x-ray pulse). Thus, we write the x-ray electric field as a slowly variant envelope times a fast oscillating term $\boldsymbol{\varepsilon}_x(t) = \mathbf{g}_x(t) \cos \omega_x t$. Due to the fact that x-ray pulses interact with inner-shell and core- orbitals, whereas IR pulses interacts with orbitals close to the valence shell, it becomes necessary rewrite the Ansatz (1) as:

$$|\psi(\mathbf{r}, t)\rangle = \sum_m \int d\mathbf{k}^3 a_g(\mathbf{k}, t)|\mathbf{k}, m\rangle + \sum_\lambda \int d\mathbf{k}^3 a_\lambda(\mathbf{k}, t)|\mathbf{k}, \lambda\rangle \tag{5}$$

(where m stands for the core- a orbitals and λ stands for the valence-shell orbitals). We rewrite the core orbital amplitudes as $a_m(\mathbf{k},t) = e^{\omega_x t} c_m(\mathbf{k},t)$, which leads to $\rho_{im} = a_i^\dagger a_m = e^{\omega_x t} a_i^\dagger c_m = e^{\omega_x t}\tilde{\rho}_{im}$. Finally, if we use the rotating-wave approximation (RWA) with these density matrix elements, we get $\boldsymbol{\varepsilon}(t)e^{\omega_x t}\tilde{\rho}_{im} \approx \boldsymbol{\varepsilon}_x(t)e^{\omega_x t}\tilde{\rho}_{im} \approx \frac{\mathbf{g}(t)}{2}\tilde{\rho}_{im}$, and assuming that $E_i(\mathbf{k}) > E_m(\mathbf{k})$, we rewrite the density matrix (4) as

$$
\begin{aligned}
i\,\dot{\rho}_{ij}(\mathbf{k},t) \quad &= [E_j(\mathbf{k}) - E_i(\mathbf{k})]\rho_{ij}(\mathbf{k},t) + i\boldsymbol{\varepsilon}_o(t)\cdot\frac{\partial}{\partial\mathbf{k}}\rho_{ij}(\mathbf{k},t) \\
&\quad + \sum_{\lambda'\neq j}\boldsymbol{\varepsilon}_o(t)\cdot\mathbf{d}_{j\lambda'}(\mathbf{k})\;\rho_{i\lambda'}(\mathbf{k},t) - \sum_{\lambda'\neq i}\boldsymbol{\varepsilon}_o(t)\cdot\mathbf{d}^*_{i\lambda'}(\mathbf{k})\;\rho_{\lambda' j}(\mathbf{k},t) \\
&\quad + \sum_{m'\neq j}\frac{\mathbf{g}_x(t)}{2}\cdot\mathbf{d}_{jm'}(\mathbf{k})\;\tilde{\rho}_{im'}(\mathbf{k},t) - \sum_{m'\neq i}\frac{\mathbf{g}_x(t)}{2}\cdot\mathbf{d}^*_{im'}(\mathbf{k})\;\tilde{\rho}_{m' j}(\mathbf{k},t) \\
i\,\partial_t\tilde{\rho}_{im}(\mathbf{k},t) &= [E_m(\mathbf{k}) - E_i(\mathbf{k}) + \omega_x]\tilde{\rho}_{im}(\mathbf{k},t) + i\boldsymbol{\varepsilon}_o(t)\cdot\frac{\partial}{\partial\mathbf{k}}\tilde{\rho}_{im}(\mathbf{k},t) \\
&\quad + \sum_{\lambda'\neq m}\frac{\mathbf{g}_x(t)}{2}\cdot\mathbf{d}_{m\lambda'}(\mathbf{k})\;\rho_{i\lambda'}(\mathbf{k},t) - \sum_{\lambda'\neq i}\boldsymbol{\varepsilon}_o(t)\cdot\mathbf{d}^*_{i\lambda'}(\mathbf{k})\;\tilde{\rho}_{\lambda' m}(\mathbf{k},t) \\
&\quad + \sum_{m'\neq m}\boldsymbol{\varepsilon}_o(t)\cdot\mathbf{d}_{mm'}(\mathbf{k})\;\tilde{\rho}_{im'}(\mathbf{k},t) - \sum_{m'\neq i}\frac{\mathbf{g}_x(t)}{2}\cdot\mathbf{d}^*_{im'}(\mathbf{k})\;\rho_{m' m}(\mathbf{k},t) \\
i\,\dot{\rho}_{nm}(\mathbf{k},t) \quad &= [E_m(\mathbf{k}) - E_n(\mathbf{k})]\rho_{nm}(\mathbf{k},t) + i\boldsymbol{\varepsilon}_o(t)\cdot\frac{\partial}{\partial\mathbf{k}}\rho_{nm}(\mathbf{k},t) \\
&\quad + \sum_{\lambda'\neq m}\frac{\mathbf{g}_x(t)}{2}\cdot\mathbf{d}_{m\lambda'}(\mathbf{k})\;\tilde{\rho}_{n\lambda'}(\mathbf{k},t) - \sum_{\lambda'\neq n}\frac{\mathbf{g}_x(t)}{2}\cdot\mathbf{d}^*_{n\lambda'}(\mathbf{k})\;\tilde{\rho}_{\lambda' m}(\mathbf{k},t) \\
&\quad + \sum_{m'\neq m}\boldsymbol{\varepsilon}_o(t)\cdot\mathbf{d}_{mm'}(\mathbf{k})\;\rho_{nm'}(\mathbf{k},t) - \sum_{m'\neq n}\boldsymbol{\varepsilon}_o(t)\cdot\mathbf{d}^*_{nm'}(\mathbf{k})\;\rho_{m' m}(\mathbf{k},t)
\end{aligned}
\tag{6}
$$

where we have split the density matrix into three parts: i) ρ_{ij} for high energy orbitals interacting with high energy orbitals, ii) $\tilde{\rho}_{im}$ for high energy orbitals interacting with low energy orbitals and iii) ρ_{ij} low energy orbitals with interacting with small energy. Note that in the previous equations we should also include the relaxation terms mentioned above.

2.1. Attosecond Transient Absorption

The x-ray absorption of the system cannot be described in the linear response limit, as the medium is interacting with a IR pulse during the response time. Hence, we use the general formula to account for the absorption of the system:

$$S(\omega) = 2\,\mathrm{Im}[\mu(\omega)E^*(\omega)] \tag{7}$$

in which the dipole is defined as $\mu(t) = q\langle\psi(t)|\mathbf{r}\cdot\hat{u}|\psi(t)\rangle$. Using Ansatz (5), we have the following expression $\mu(t) = q\langle\psi(t)|\mathbf{r}\cdot\hat{\mathbf{u}}|\psi(t)\rangle \approx q\left[\sum_{\lambda m'}\int d\mathbf{k}^3\tilde{\rho}_{m'\lambda}(\mathbf{k},t)d_{m'\lambda}(\mathbf{k})e^{-i\omega_x t} + c.c.\right]$. Since we are interested in the x-ray absorption of the pulse, we only consider the main contributions to those transitions (i.e. λm contributions). Now if we perform the Fourier transform of this term, a fast rotating and a slow rotating term arise. Within the RWA, we neglect the fast rotating term and obtain: $\mu(\omega) \approx q\int dt\left[\sum_{\lambda m'}\int d\mathbf{k}^3\tilde{\rho}_{m'\lambda}(\mathbf{k},t)d_{m'\lambda}(\mathbf{k})\right]e^{i(\omega-\omega_x)t}$. We perform similarly the Fourier transform of the electric field: $E(\omega) \approx \int dt\frac{g_x(t)}{2}e^{i(\omega-\omega_x)t}$. Finally, the ATA centered around the frequency ω_x is given by

$$S(\omega+\omega_x) = 2\mathrm{Im}\left[\mu(\omega+\omega_x)E^*(\omega+\omega_x)\right] \approx 2\mathrm{Im}\left[q\int dt\left[\sum_{\lambda m'}\int d\mathbf{k}^3\tilde{\rho}_{m'\lambda}(\mathbf{k},t)d_{m'\lambda}(\mathbf{k})\right]e^{i\omega t}\cdot\int dt\frac{g_x(t)}{2}e^{-i\omega t}\right] \tag{8}$$

3. Computational Data

To solve equations (6), we have implemented in C++ the well-known 4^{th}-order Runge-Kutta method [6]. To help the implementation of this numerical solution, it is convenient to rewrite the density matrix elements obtained in the previous section in the hole formalism: what we solve in our calculations is the hole creation and annihilation due to the action of the pulses, which is equivalent to electron excitation and de-excitation respectively [5]. For describing pump-probe experiments, we need to consider that both pulses are well separated in frequency, which raises a time integration problem: the low frequency makes the time integration to be long, and the small frequency makes small the time resolution. If the x-ray is not far from resonance and the intensity is not strong enough, this problem can be solved by imposing the RWA to the x-ray pulse avoiding small time step resolution. Also, in order to renormalize the intraband couplings and avoid derivative with respect to the quasi momenta, we transform the semiconductor Bloch equations into the laser-dressed quasi-continua in the presence of an IR field [7].

3.1. Three-band Model

The first goal is to use the developed theoretical approach to understand x-ray ATA in semiconductor materials and to find its connection with the induced electron dynamics. For the sake of simplicity, we start with a simple model where the semiconductor band structure has been simplified. The results obtained with this model, can be used in the understanding and future development of fuller models for real semiconductors.

Our simple model is based on three 1D bands that are needed to study the transient absorption: core-hole band, valence band and conduction band. The core-hole band is introduced to study the x-ray absorption, this is coupled with the valence and the conduction band. On the other hand, valence and conduction band are coupled via the IR pulse. The lattice parameter a is given by $a = 5.32$ a.u., and the energy gap at the Γ-point is $E_0 = 0.057$ a.u. (1.55 eV). The structure of the valence and conduction band is showed in figure 2. Core-hole band is placed deep down at -16 a.u. (-435 eV) energy. In addition to the three-band model, we also implemented a three-level system for an atomic system, to compare the results with our semiconductor model. The core level has the same energy (-16 a.u.), and the resonance frequency of the transition between the ground state and the excited state is $\omega_0 = 0.057$ a.u., the same than the energy gap of the three-band model.

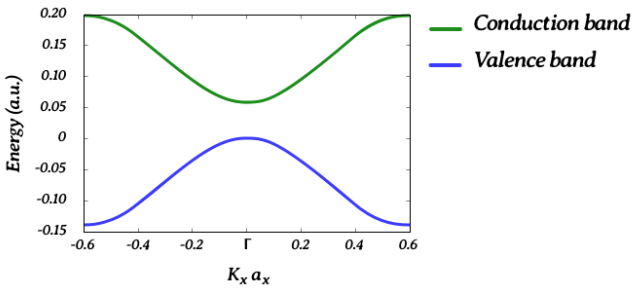

Figure 2. Brillouin zone of the outer-band structure of our three-band model. We have an interval from $-\pi/a$ to π/a with Nkx=500 points and a step of dkx=0.0024 with a Γ-point value of $E_0 = 0.057$ a.u. (1.55 eV). Core-hole band is not shown.

3.2. Simulation data

In ATA experiments, both IR and x-ray pulses are ultrashort, i.e. pulse lengths of hundreds of attosecond to few femtoseconds. We model our pulses with Gaussian profiles. For the IR frequency, the Gaussian pulse is characterized for having a $\text{FWHM}_{\text{intensity}} = 9.97$ fs, and being

polarized in the $\hat{z}$ direction. We have performed our simulations considering an IR-frequency of $\omega_0 = 0.057$ a.u. ($\lambda_0 = 800\ nm$, 1.55 eV), resonant with the transition between gs and es of the three-level atom and with the bandgap of the three-level model, and an IR-frequency of $\omega_1 = 0.047$ a.u. ($\lambda = 970$ nm, 1.28 eV), non-resonant with either the atom transition or any point of the three-band model. Regarding the x-ray pulse, it is also polarized in the $\hat{z}$ direction and presents a sigma of $\mathrm{FWHM}_{\mathrm{intensity}} = 0.33$ fs. The frequency of the pulse is $\omega_x = 16$ a.u. ($\lambda = 2.85$ nm), being the central frequency resonant with the ground-state of the atom model and located just above the valence band. In any case, due to the broad bandwidth of the pulse, this excites both the valence and the conduction bands. The dipole that couples the different bands have the following values: 1.46 a.u. for the IR-coupling between valence and conduction band, 0.0010 a.u. for the x-ray coupling of the core-hole and valence band, and 0.0009 a.u. for the x-ray coupling between core-hole and conduction band.

When we consider Gaussian pulsed lasers in a two-level atom, the excitation is proportional to $|\sin(\Theta/2)|^2$, and the dimensionless parameter is defined as

$$\Theta = \left| \frac{\mu_{12}}{\hbar} \int_{-\infty}^{+\infty} \varepsilon_o(t) dt \right| = \frac{(2\pi)^{1/2} \mu_{12} \cdot \sigma \cdot \varepsilon_0}{\hbar} \tag{9}$$

where μ_{12} is the dipole moment between the two levels coupled by the IR pulse, σ is the broadening of the Gaussian pulse, and ε_0 is the peak amplitude [8]. This is a resemblance of the formula for the Rabi oscillations in a two-level system, in which the parameter (9) plays the same role as Ω_Rt, where Ω_R is the Rabi frequency. We fix the field intensities in our simulations in order to have π ($\mathrm{I} = 4.28 \cdot 10^{11}$ W/cm^2), 2π ($\mathrm{I} = 1.71 \cdot 10^{12}$ W/cm^2), 3π ($\mathrm{I} = 3.86 \cdot 10^{12}$ W/cm^2) and 4π ($\mathrm{I} = 6.86 \cdot 10^{12}$ W/cm^2) pulses (in the atomic system reference).

Given all these considerations we will perform simulations of pump-probe experiments with delays from -21 fs to 21 fs, to study three physical scenarios: a three-level atomic system, a semiconductor without considering intraband interactions, and a semiconductor considering all interactions. For each case, we consider field intensities corresponding to the values indicated above.

4. Results

From the simulations we are able to get information about the electron population in the bands close to the Fermi level as well as the calculation of the ATA spectra to be measured in the experiment. To calculate ATA spectra, we calculate the absorption of the x-ray probe pulse with and without the IR pump pulse. In the following, we study ω_0 (0.057 a.u.) simulations and ω_1 simulations (0.047 a.u.) for the three different systems under investigation.

4.1. Atomic System

The simplest case in the study of the x-ray ATA absorption is the atomic system. We see in figure 3, the sequence of figures for the π, 2π, 3π and 4π pulses. Figures corresponding to population dynamics at ω_0 (figure 3 (a), (b), (c), (d) top figures) allow us to observe the characteristic Rabi oscillations of resonant transitions. Population oscillates according to the induced cycle π: even cycles give rise to complete oscillations (figure 3 (b), (d) top figures), whereas for odd cycles the last oscillation is not complete (3 (a), (c) top figures). When the IR frequency is ω_1 (figure 3 (e), (f), (g), (h) top figures), we observe how Rabi oscillations change its frequency, being reduced the population transfer. This result is caused by the detuning between the central frequency of the IR

pulse and the resonant frequency of the atom, which gives rise to faster oscillations and reduces the maximum transfer of carriers between the ground state and the excited state.

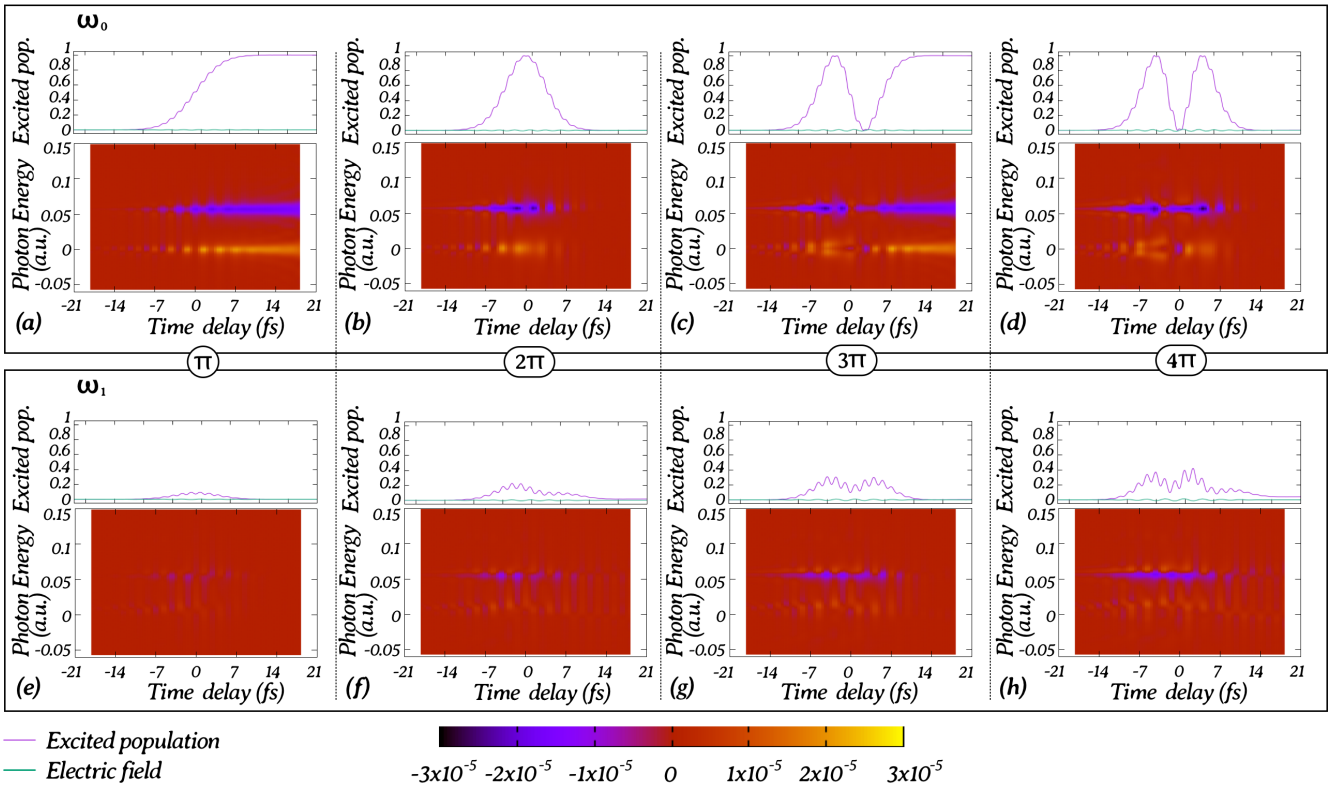

Figure 3. Atomic Model: Population in time in the valence and conduction band (top figures), and ATA spectra (bottom figures). Figures correspond to ω_0 case: **(a)** π pulse **(b)** 2π pulse **(c)** 3π pulse **(d)** 4π pulse. For ω_1 case: **(e)** π pulse **(f)** 2π pulse **(g)** 3π pulse **(h)** 4π pulse

Now we analyze the ATA spectra corresponding to these physical scenarios (figure 3 (a), (b), (c), (d) bottom figures). Due to Pauli principle exclusion, the promotion of the electrons to the conduction band by the absorption of IR photons would block the promotion of electrons from the core-hole band to the conduction band. However, holes are created in the valence band, opening the possibility of core electrons to be excited into these. Within this context, Rabi oscillations are observed in the ATA spectra at ω_0 during the presence of the IR pulse. For odd cycles (figure 3 (a), (c) bottom figures), electron remains in the excited level, which is clear in the ATA spectrum. For even cycles (figure 3 (b), (d) bottom figures), light absorption in the conduction band reachs a minimum at the maxima of the Rabi oscillations, and then it comes back to a higher absorption. In the valence band the effects observed are the opposite, and the maxima of the Rabi oscillations indicate maximum light absorption in this band. This can be read as a promotion of electrons from the core-hole band to the valence band. Similarly, we also observe the out-of-phase oscillations in the case of the non-resonant pulse(figure 3 (e), (f), (g), (h) bottom figures). This shows the potential of ATA to unveil the fast electron dynamics induced by the ultrashort IR pulse.

4.2. Semiconductor with no intraband interactions

In terms of complexity, the following system to study is a semiconductor in which intraband interactions are neglected. As a consequence, we expect a response similar to a collective of two-level systems with different energy gap. The results are presented in figure (4).

If we focus on the case with IR-frequency ω_0, in particular on the population dynamics (figure 4 (a), (b), (c), (d) top figures), we observe how population performs the same Rabi oscillations as in the atom case, but proportionally it is much less transferred, and presents different peaks which break the smoothness observed in the atom case. This occurs because the semiconductor model is a reciprocal lattice in which each point presents a particular transition energy. Consequently, we have only one point (Γ-point) that oscillates at resonance, and a few points that oscillate close to resonance. The joint oscillation of these points is responsible of the Rabi oscillations observed, whereas the oscillation of the points far from resonance contributes to the broadening of the peaks and to reduce transfer population.

In the ATA spectra, light absorption is much more intense in the valence band, as well as the blocking of electron promotion in the the conduction band. This is due to the fact that we have a reciprocal lattice with many carriers involved contributing to light absorption. At ω_o frequency (figure 4 (a), (b), (c), (d) bottom figures), Rabi oscillations are observed as in the previous model, performing the same oscillations for π odd and even pulses. Following Rabi oscillations is not so clear though, because despite of having more absorption, contribution of the far from resonance points of the reciprocal lattice generate extra oscillations in the ATA profile. When the IR frequency is equal to ω_1 (figure 4 (e), (f), (g), (h) bottom figures), the total contribution of the reciprocal space carriers does not make possible the observation of Rabi oscillations. Instead, what we observe are low (high) absorption regions at the center of the pulse in the conduction (valence) band, which disappear at the end of the pulse. This result can be understood as an electron promotion from valence to conduction band at the maximum of the IR-pulse via electron

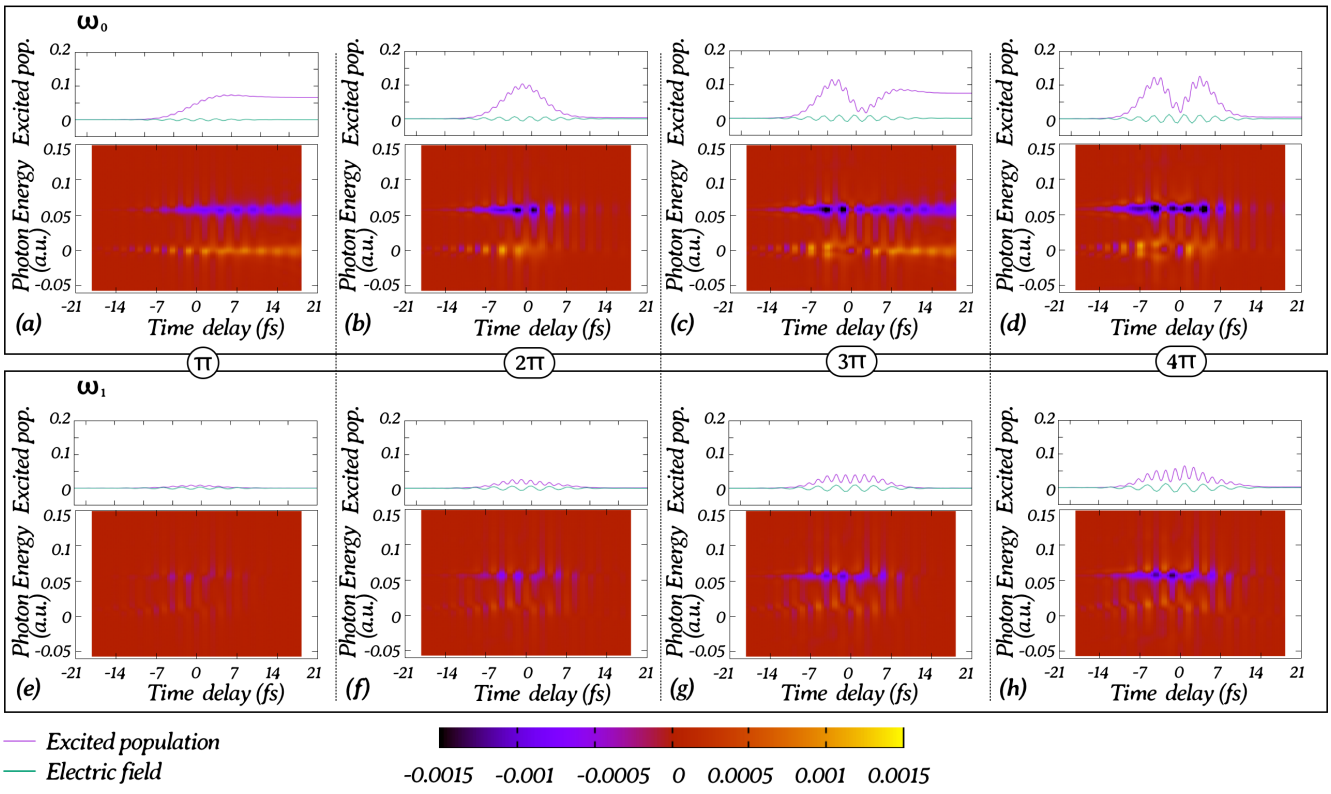

Figure 4. Semiconductor with no intraband interactions: Population in time in the valence and conduction band (top figures), and ATA spectra (bottom figures). Figures correspond to ω_0 case: **(a)** π pulse **(b)** 2π pulse **(c)** 3π pulse **(d)** 4π pulse. For ω_1 case: **(e)** π pulse **(f)** 2π pulse **(g)** 3π pulse **(h)** 4π pulse

tunneling, followed by a return of the electrons at the end of the pulse.

4.3. Semiconductor with interband interactions

We are ready to study the case of a semiconductor in which all the interactions (intraband and interband) are considered, see figure 5. Here, the reciprocal lattice behaves as oscillators with different resonant energy, but in this case the points of the lattice interact between them via intraband interactions.

For ω_0 frequency, the population in time show us half a cycle of the Rabi oscillation for a π pulse (figure 5 (a) top figure). If we increase the intensites to values corresponding to 2π, 3π, 4π (figure 5 (b), (c), (d) respectively, top figures), we can see how the Rabi oscillations observed in the previous cases disappear, and what we simply obtain is a continuous population transfer from valence to conduction band. At high intensities, the fact that electron can move along an energy band due to intraband interactions introduce a decoherence that breaks the Rabi oscillations. In ATA spectra, the π pulse (figure 5 (a), bottom figure) is similar to the non-intraband case, but at higher intensities(figure 5 (b), (c), (d) bottom figures) we observe high absorption areas at the center of the IR pulse followed by a constant absorption.

For ω_1 frequency, the population in time and the ATA spectra show the same changes as in the ω_0 case for high intensities (figure 5 (f), (g), (h) bottom figures). In this case it is not straightforward to read the spectra, given that intraband contribution allow the movement of core electrons after being promoted into the conduction band, which give rise to a temporal change in

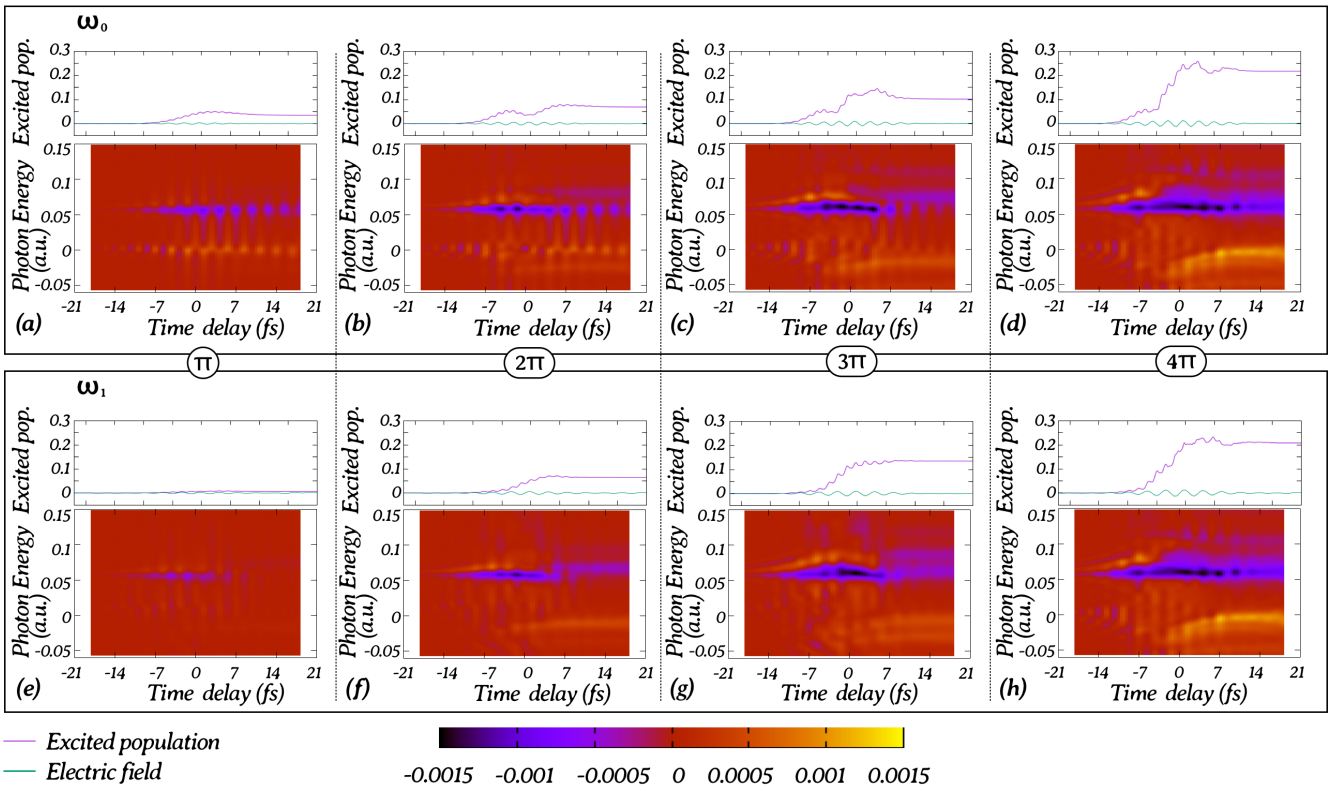

Figure 5. Semiconductor with no intraband interactions: Population in time in the valence and conduction band (top figures), and ATA spectra (bottom figures). Figures correspond to ω_0 case: **(a)** π pulse **(b)** 2π pulse **(c)** 3π pulse **(d)** 4π pulse. For ω_1 case: **(e)** π pulse **(f)** 2π pulse **(g)** 3π pulse **(h)** 4π pulse

the energy of the carriers. This introduces a new effect, interpreted as a dynamical Stark shift, that must be taken into account together with Pauli exclusion, which was the dominant effect in the previous case. This Stark shift effect explains the positive absorption in the conduction band observed in the ATA spectra at high intensities. This shows the complexity of interpreting ATA spectra that reflects attosecond dynamics and the necessity of providing theoretical modeling for the understanding of real semiconductor materials.

5. Conclusions

In conclusion, we develop the equations that describes the dynamics of an attosecond pump-probe experiment, being the probe an x-ray attosecond pulse, as well as the calculation of ATA spectra. We implement a 4^{th}-order Runge-Kutta method to obtain the numerical solution of these equations. In this manuscript we study two simplified 1D physical models: a three-level atom model, and a three-band semiconductor model. We have the possibility to turn on and off the intraband interactions of the semiconductor model, allowing to inspect and obtain a deeper insight of the physical mechanisms. By performing simulations at different IR-frequencies and intensities, we unveil several effects. In the atomic model, the results of the population dynamics and the ATA spectra allows to observe Rabi oscillations for resonant and non-resonant transitions, and to study the role of the Pauli principle exclusion in the electron transfer between the different atomic levels considered. In the case of the semiconductor model with no intraband interactions, the effects can be interpreted as a collective of the atomic model, but each independent k-point of the band we have different energy dispersion with produces a different contribution to the coherent oscillation. As a result, less population is transferred and a broadening of the Rabi oscillations peaks is observed. If intraband interactions are considered, at high IR intensities, a dynamical Stark shift effect appears and breaks the coherence of the oscillations observed in the previous cases. The results of this work can be extended to real semiconductor models. Further investigation is needed to understand future ATA studies in semiconductors, an essential technique that allows us to glimpse the fast dynamics of electrons with unprecedented temporal resolution.

Acknowledgements

I would like to thank Dr. Antonio Picón for his guidance and support in the development of this project. I would also like to thank Prof. Dr. Jens Biegert for fruitful discussion and giving me the opportunity of doing the master thesis project in his group.

References

[1] A. H. Zewail, J. Phys. Chem. A **104**, 5660-5694 (2000).
[2] S. R. Leone and D. M. Neumark, Faraday Discuss., **194**, 15-39 (2016).
[3] S. M. Teichmann, F. Silva, S. L. Cousin, M. Hemmer, and J. Biegert, Nature Commun. **7**, 11493 (2016).
[4] M. Nisoli, P. Decleva, F. Calegari, A. Palacios, and F. Martín, Chem. Rev. **117**, 10760-10825 (2017).
[5] H. Haug and S. W. Koch, *Quantum Theory of the Optical and Electronic Properties of Semiconductors*, World Scientific (New Jersey, 2004).
[6] B. P. Flannery, S. A. Teukolsky, W. H. Press, and W. T. Vetterling, *Numerical Recipes in C*, Cambridge University Press (Cambridge, 2007).
[7] G. Vampa, C. R. McDonald, G. Orlando, D. D. Klug, P. B. Corkum, and T. Brabec, Phys. Rev. Lett. **113**, 073901 (2014).
[8] M. Fox, *Quantum Optics: An Introduction*, Oxford University Press (US, 2006)